Navigating contradictions: Salmonella Typhimurium chemotactic responses to conflicting effector stimuli

Kailie Franco [1], Zealon Gentry-Lear [2], Michael Shavlik [3], Michael J. Harms [2,3], and Arden Baylink [1*]

[1] Washington State University, Department of Veterinary Microbiology and Pathology, Pullman, WA 99164

[2] University of Oregon, Institute of Molecular Biology, Eugene, OR, 97403

[3] University of Oregon, Department of Chemistry & Biochemistry, Eugene, OR, 97403

[*] Corresponding author: arden.baylink@wsu.edu (A. Baylink)

Summary

Chemotaxis controls swimming motility and colonization of many intestinal bacteria, but how enteric pathogens navigate the complex chemical landscape of the gut, which contains contradictory chemoattractant and chemorepellent stimuli, remains poorly understood. We find *Salmonella* Typhimurium requires chemotactic sensing of two opposing signals present in the intestinal lumen—the microbiota metabolite and bacteriostatic chemorepellent indole, and the nutrient chemoattractant L-Ser—for efficient invasion of colonic tissue. Despite feces being the major biological source of indole, accumulating to millimolar levels, non-typhoidal *Salmonella* are strongly attracted to fecal material because chemoattraction to L-Ser and other attractants override indole chemorepulsion. This behavior is orchestrated through the chemoreceptor Tsr, which coordinates a spectrum of distinct rearrangements in the bacterial population structure based on the ratio of L-Ser to indole. Through seeking niches with the highest L-Ser to indole ratio, *S.* Typhimurium presumably optimizes nutrient access and avoids regions of high-competitor density.

Keywords:

Chemotaxis, *Salmonella*, chemoeffector, chemohalation, serine, indole, chemoreceptor, Tsr, microbiome, gastrointestinal pathogen

Introduction

Many bacteria that colonize the gastrointestinal tracts of humans and other animals employ chemotaxis to sense chemical effectors in the gut lumen and swim to environments conducive for growth and colonization [1–5]. Chemotaxis enables motile bacteria to seek nutrients, avoid toxins, and respond to molecular cues [1,2,4,5]. This process is controlled by chemoreceptor proteins, which recognize chemical effectors and transduce signals through a phosphorylation cascade to regulate flagellar rotation and swimming direction, ultimately determining the spatial and temporal patterns of bacterial colonization (Fig. 1A) [1,2,6,7]. While many effectors have been studied and characterized in isolation as attractants or repellents [4,7], natural environments contain mixtures of opposing signals. In the enteric lumen, bacteria encounter a complex milieu of conflicting effector signals, and little is known about how they prioritize these signals to direct their movement and colonization (Fig. 1B). Ultimately, the colonization topography of bacteria within the gut influences the health of the host through nutrient absorption, developmental regulation, and resistance to pathogens [8–10].

A chemical effector of major importance for enteric bacterial communities is indole, an interbacterial signaling molecule that regulates diverse aspects of bacterial physiology and lifestyle [11–13]. Indole is excreted by gut microbiota as a byproduct of tryptophan metabolism and accumulates to millimolar levels in human feces (Fig. 1A-B) [11,14,15]. Indole is amphipathic and can transit bacterial membranes to regulate biofilm formation and motility, suppress virulence programs, and exert bacteriostatic and bactericidal effects at high concentrations [11–13,15–17]. Indole was one of the earliest identified chemorepellents, and subsequent work has extensively explored its role in *Escherichia coli* chemotaxis (Table S1) [13,18–22]. The molecular mechanism by which *E. coli* senses indole remains unclear, but is known to involve the chemoreceptor taxis to serine and repellents (Tsr) (Fig. 1A-B) [18,20,21]. From this body of work, the hypothesis emerged that indole repels pathogens and restricts their growth as a mechanism of colonization resistance conferred by the microbiota [11–13,18,23]. However, no prior work has actually tested whether human fecal material, the major biological source of indole in the gut, which contains a complex mixture of effectors, induces chemorepulsion or inhibits pathogen growth at physiologically relevant levels.

We were interested in further studying the role of Tsr in navigating contradicting effector stimuli because this chemoreceptor has an interesting dual function: it both senses chemorepellents and also recognizes the amino acid and nutrient, L-Ser as a chemoattractant (Fig. 1A-B) [1,24–26].

Prior *in vitro* work with purified effectors showed that when both attractants and repellents are present, Tsr facilitates "intermediate" responses between chemoattraction and chemorepulsion, suggesting that, in some cases, navigating conflicting chemotactic stimuli is regulated at the single chemoreceptor level [20,21]. The mechanisms and temporal dynamics of these intermediate chemotactic behaviors are mostly uncharacterized, but could be relevant in natural settings that contain conflicting effectors. We recently reported that many enteric pathogens and pathobionts possess Tsr orthologues, including the genera *Salmonella*, *Citrobacter*, and *Enterobacter* [24]. Whether these and other bacteria respond to indole as a chemorepellent has remained unclear because all prior studies of indole taxis focused on *E. coli* (Table S1).

Salmonella Typhimurium is a frank pathogen that relies on chemotaxis for enteric invasion [27–30], and differs fundamentally from *E. coli* because it lacks tryptophanase genes and cannot itself produce indole, which could provide a novel perspective on indole taxis [31,32]. In this study, we used the pathogen *S.* Typhimurium as a model to: (1) test the hypothesis that the microbiota secretion product indole is protective against enteric invasion, (2) investigate if pathogens are repelled by indole-containing fecal material, and (3) examine how the chemoreceptor Tsr regulates pathogen spatial localization in response to conflicting chemotactic stimuli of the intestinal environ. Our study is the first to employ live imaging to directly visualize how enteric pathogen populations dynamically restructure in response to physiological mixtures of attractants and repellents. We demonstrate that the ability to navigate conflicting effector signals in fact mediates efficient pathogen invasion, and that chemotaxis responses to natural biological combinations of effectors and their impacts on infection outcomes, are not easily predicted based on responses to individual effectors.

Results & Discussion

Opposing chemoeffector stimuli mediate efficient pathogen invasion in swine colonic explants

We sought to determine whether indole in human fecal matter protects against *S.* Typhimurium infection and whether this involves chemotaxis mediated by the chemoreceptor Tsr. To address this, we developed a swine colonic explant model that mimics the architecture and size of adult human colonic tissue [33–37]. The explant tissue was gently cleaned and treated with various effector solutions: solubilized human feces, purified indole and/or L-Ser at fecal-relevant

concentrations, or buffer as a control (see Method Details). The tissue was then exposed to co-infection with wild-type (WT) *S.* Typhimurium strain IR715 and either a *cheY* mutant (motile but non-responsive to chemoeffector stimuli) or a *tsr* deletion mutant (Fig. 1C-D, Key Resources Table) [28]. To assess the role of chemotaxis in infection, we quantified total bacteria harvested from tissue homogenates and enumerated intracellular bacteria using a gentamicin wash at 1-, 3-, and 6-h post-infection (Fig. 1C, Method Details) [38,39]. For buffer-treated explants, WT *S.* Typhimurium showed a modest time-dependent advantage in colonization and invasion compared to chemotactic mutants, indicating that chemotaxis, and specifically Tsr, promotes tissue colonization under baseline conditions (Fig. 1E, Fig. S1A-B).

Contrary to the hypothesis that indole-rich fecal matter would inhibit pathogen colonization, we found that fecal treatment significantly enhances intracellular invasion of WT *S.* Typhimurium, providing a >100-fold competitive advantage mediated by Tsr (Fig. 1F, Fig. S1C-D). Analysis of the liquified human fecal matter used in this study revealed an indole concentration of 862 µM, consistent with previously reported ranges (0.5–5 mM) (Fig. 1D, Method Details) [11,14–17]. However, when colonic tissue was treated with purified indole at the same concentration, the competitive advantage of WT over the chemotactic mutants was abolished (Fig. 1G, Fig. S1E-F). Given that Tsr mediates attraction to L-Ser in both *E. coli* and *S.* Typhimurium, we hypothesized that L-Ser present in feces might be responsible for increased colonization of fecal-treated tissue [1,24,40,41]. However, treatment with 338 µM L-Ser, the concentration present in our fecal sample (Fig. 1D, Method Details), actually reduces the competitive advantage of WT bacteria, similar to the effect of indole alone (Fig. 1H). While treatments with either indole or L-Ser alone reduce the WT advantage, total bacterial loads are similar, suggesting that neither effector is "protective" in terms of total infection burden (Fig. S1). We then wondered whether Tsr might require sensing of both indole and L-Ser in combination to coordinate infection. Interestingly, we found that treatment containing a mixture of indole and L-Ser restores the competitive advantage of WT (Fig. 1I, Fig. S1I-J). Thus, we discovered that fecal material, the major biological source of indole in the gut, does not protect against *S.* Typhimurium invasion, and that the fecal effectors indole and L-Ser, in combination, direct efficient colonic invasion through chemotaxis and the chemoreceptor Tsr (Fig. 1, Fig. S1).

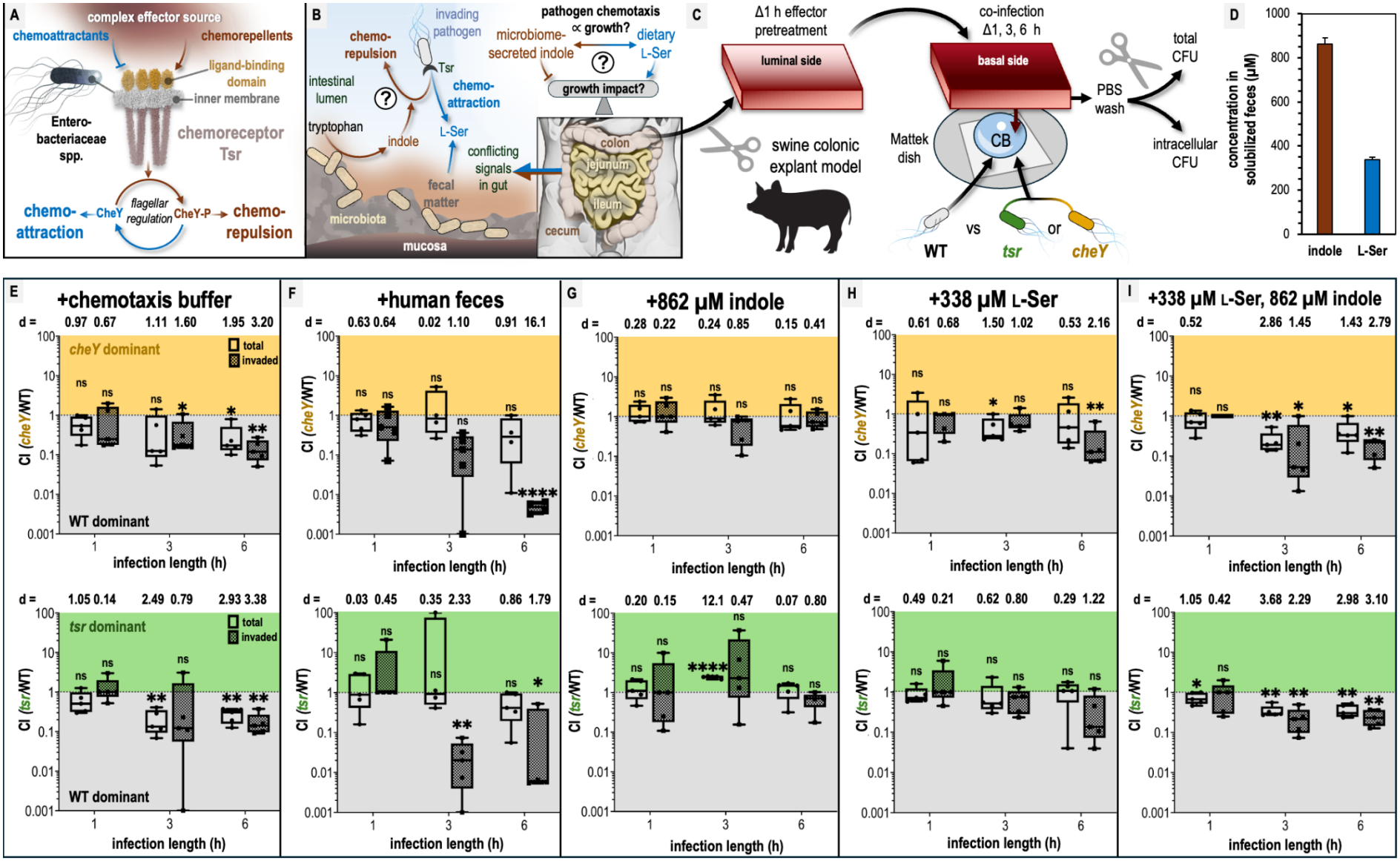
A
complex effector source
chemoattractants
chemorepellents
ligand-binding domain
inner membrane
Entero-bacteriaceae spp.
chemoreceptor Tsr
chemo-attraction
CheY
flagellar regulation
CheY-P
chemo-repulsion
B
invading pathogen
chemo-repulsion
Tsr
chemo-attraction
intestinal lumen
tryptophan
indole
L-Ser
conflicting signals in gut
fecal matter
microbiota
mucosa
pathogen chemotaxis
microbiome-secreted indole
∝ growth?
dietary L-Ser
growth impact?
colon
jejunum
ileum
cecum
C
Δ1 h effector pretreatment
luminal side
swine colonic explant model
co-infection Δ1, 3, 6 h
basal side
Mattek dish
CB
PBS wash
total CFU
intracellular CFU
WT
vs
tsr
or
cheY
D
concentration in solubilized feces (μM)
indole
L-Ser
E
+chemotaxis buffer
F
+human feces
G
+862 μM indole
H
+338 μM L-Ser
I
+338 μM L-Ser, 862 μM indole
cheY dominant
tsr dominant
total
invaded
WT dominant
CI (cheY/WT)
CI (tsr/WT)
infection length (h)

123

Fig. 1. Tsr and chemotaxis mediate efficient pathogen invasion of colonic tissue in the presence of conflicting chemotactic stimuli. A-B. Overview of the role of Tsr in chemotactic responses and premise of this study. C. Experimental design of colonic explant infections. D. Serine (presumed to be nearly 100% L-Ser, see Materials & Methods) and indole content of liquid human fecal treatments. E-I. Competitive indices (CI) of colony-forming units (CFU) recovered from co-infected swine explant tissue, either from the total homogenate (open box and whiskers plots), or the invaded intracellular population (checkered box and whisker plots), as indicated (n=5). Boxes show median values (line) and upper and lower quartiles, and whiskers show max and min values. Effect size (Cohen's *d*) and statistical significance are noted (not significant, ns; * $p < 0.05$, ** $p < 0.01$, *** $p < 0.001$, **** $p < 0.0001$). See also Figure S1.

Non-typhoidal S. enterica are attracted to human feces despite high indole content

Having found that Tsr mediates colonic invasion for *S.* Typhimurium, we next sought to learn what chemotactic behaviors this chemoreceptor orchestrates in response to human fecal material; given the high concentration of indole, we expected to observe chemorepulsion based on earlier studies of Tsr function in *E. coli* (Fig. 1D, Table S1) [18–21]. We employed the chemosensory injection rig assay (CIRA) for live-imaging of bacterial chemotaxis responses to a source of effectors injected through a glass microcapillary [24]. In this assay, chemoattraction is observed as an influx of cells toward the effector source and chemorepulsion as decreasing cells (Figure S2). As described previously, effector injection introduces a steep microgradient, and using mathematical modeling of the diffusion of the fecal sources of indole and L-Ser, we can approximate the local concentrations experienced by bacteria at a given distance from the injection source, which for most of the field of view is in the picomolar to low nanomolar range (Fig. 2A, Method Details) [24].

Over five minutes, we found both WT and *tsr* exhibit strong chemoattraction to fecal material, whereas *cheY* remains randomly distributed (Fig. 2B, Movie S1). By examining the radial distribution of the bacterial populations, we found WT more tightly centers around the treatment source than *tsr* (Fig. 2C-E, Movie S1). In terms of the rate of accumulation of bacteria at the treatment source, the chemoattraction of *tsr* lags behind the WT for the first 120 s (Fig. 2F-G, Movie S1). We wondered how these deficiencies in fecal attraction might translate to direct competition, where different strains are experiencing the same treatment source simultaneously. To address this, we performed CIRA with solubilized human feces and two strains present in the same pond, which we tracked independently through fluorescent markers (Fig. 3). As expected, WT shows a strong chemoattraction response versus *cheY* (Fig. 3A, Movie S2). Interestingly, we found that when competed directly, WT vastly outperforms *tsr*, with the maximal bacterial distribution in proximity to the treatment source higher by about 4-fold (Fig. 3B, Movie S2).

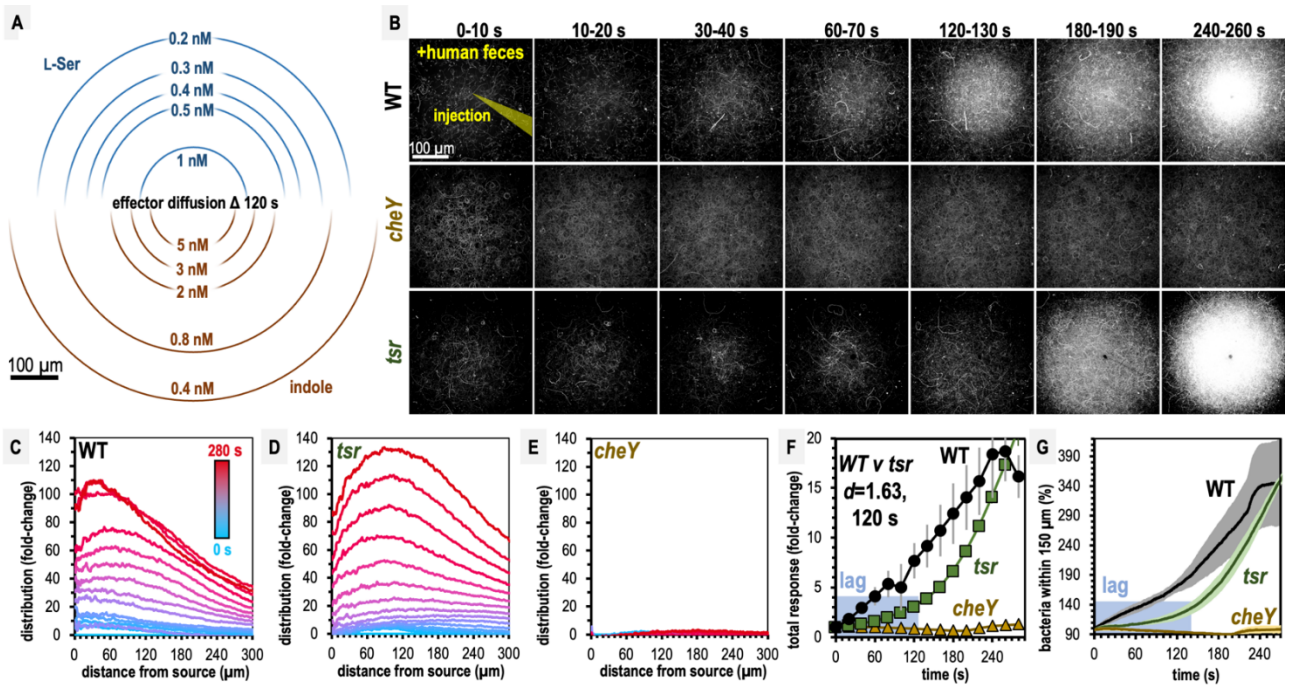

Fig. 2. *Salmonella* Typhimurium exhibits attraction toward liquid human fecal material. A. Diffusion modeling showing calculated local concentrations in CIRA experiments with liquid human fecal material. B. Max projections of representative *S.* Typhimurium IR715 responses to a central source of liquid human fecal material. C-E. Mean bacterial distribution at 10 s intervals. F-G. Temporal analyses of area under the curve (AUC) or relative number of bacteria within 150 µm of the source. Effect size (Cohen's *d*) comparing responses of WT and *tsr* attraction at 120 s post-treatment is indicated. Data are means and error bars are standard error of the mean (SEM, n=3-5). See also Movie S1, Table S1 and Figure S2.

These data confirm that despite its high indole content, *S.* Typhimurium is attracted to human fecal material through chemotaxis, and this response involves Tsr, although not as the sole mediator. We expect the attraction of the *tsr* mutant is explained by the fact that *S.* Typhimurium possesses other chemoreceptors that detect glucose, galactose, and L-Asp as chemoattractants, which are present in human feces [1,7,42–45].

To understand the broader relevance of these behaviors to enteric infections, we examined chemotaxis responses to fecal material among diverse *Salmonella* serovars and strains responsible for human infections. Using dual-channel imaging, we compared *S.* Typhimurium IR715 with a clinical isolate of *S.* Typhimurium, SARA1, and found both strains exhibit fecal attraction, although SARA1 shows a slightly weaker response (Fig. 3C, Movie S3). We then tested a clinical isolate of *S.* Newport, an emerging cause of salmonellosis in the United States and Europe [46,47]. This strain is strongly attraction to fecal material, with a tighter accumulation of cells at the

treatment source than *S.* Typhimurium IR715 (Fig. 3D, Movie S3). Lastly, we examined a clinical isolate of *S.* Enteritidis, a zoonotic pathogen commonly transmitted from poultry, which displays weak attraction to fecal material (Fig. 3E, Movie S3) [47]. Overall, we found that chemoattraction to fecal material is conserved among non-typhoidal *Salmonella* serovars responsible for human infections, although the degree of attraction varies. Notably, despite the high indole content in feces, none of the strains tested exhibit chemorepulsion.

Mediation of opposing chemotactic responses by Tsr

We wondered if our inability to observe repulsion from fecal material might be due to *S.* Typhimurium not sensing indole as a chemorepellent since this chemotactic response has only been previously described for *E. coli* (Table S1). We again employed CIRA to address this question, comparing chemotaxis responses to either 5 mM L-Ser or 5 mM indole, and found that *S.* Typhimurium responded rapidly to these two effectors as chemoattractants and chemorepellents, respectively (Fig. S2H-I). Treatment with 5 mM indole, a concentration at the upper end of what occurs in the human gut [17], induces rapid chemorepulsion with the bacteria vacating the region proximal to the source (Fig. S2B). Interestingly, the chemorepulsion response occurs faster than chemoattraction, with a zone of avoidance clearly visible within the first 10 s of indole exposure (Fig. S2I, Movie S4).

We next wondered if perhaps our fecal treatments contained insufficient indole to elicit chemorepulsion from *S.* Typhimurium. To identify the effective source concentrations that drive indole chemorepulsion and understand the temporal dynamics of this response, we performed a titration of indole across 0.05-10 mM (Fig. 3F). At all concentrations tested, indole induces chemorepulsion, and the bacteria avoid the treatment source for the duration of the 5-minute experiment (Fig. 3F-G). At source concentrations exceeding 3 mM, essentially all motile cells vacate the field of view within 60 s (Fig. 3F-G). Integrating these chemorepulsion responses and fitting them to a Monad curve suggests an indole source concentration of approximately 67 μM is sufficient for half-maximal ($K_{1/2}$) chemorepulsion (Fig. 3H). These data show that even though we observed a strong chemoattraction response to fecal material, indole at the concentration present in fecal material, and far lower, is indeed a strong chemorepellent for *S.* Typhimurium.

Based on its function in *E. coli*, we hypothesized that both indole chemorepulsion and L-Ser chemoattraction for *S.* Typhimurium could be partly or fully mediated through Tsr [7,18,26].

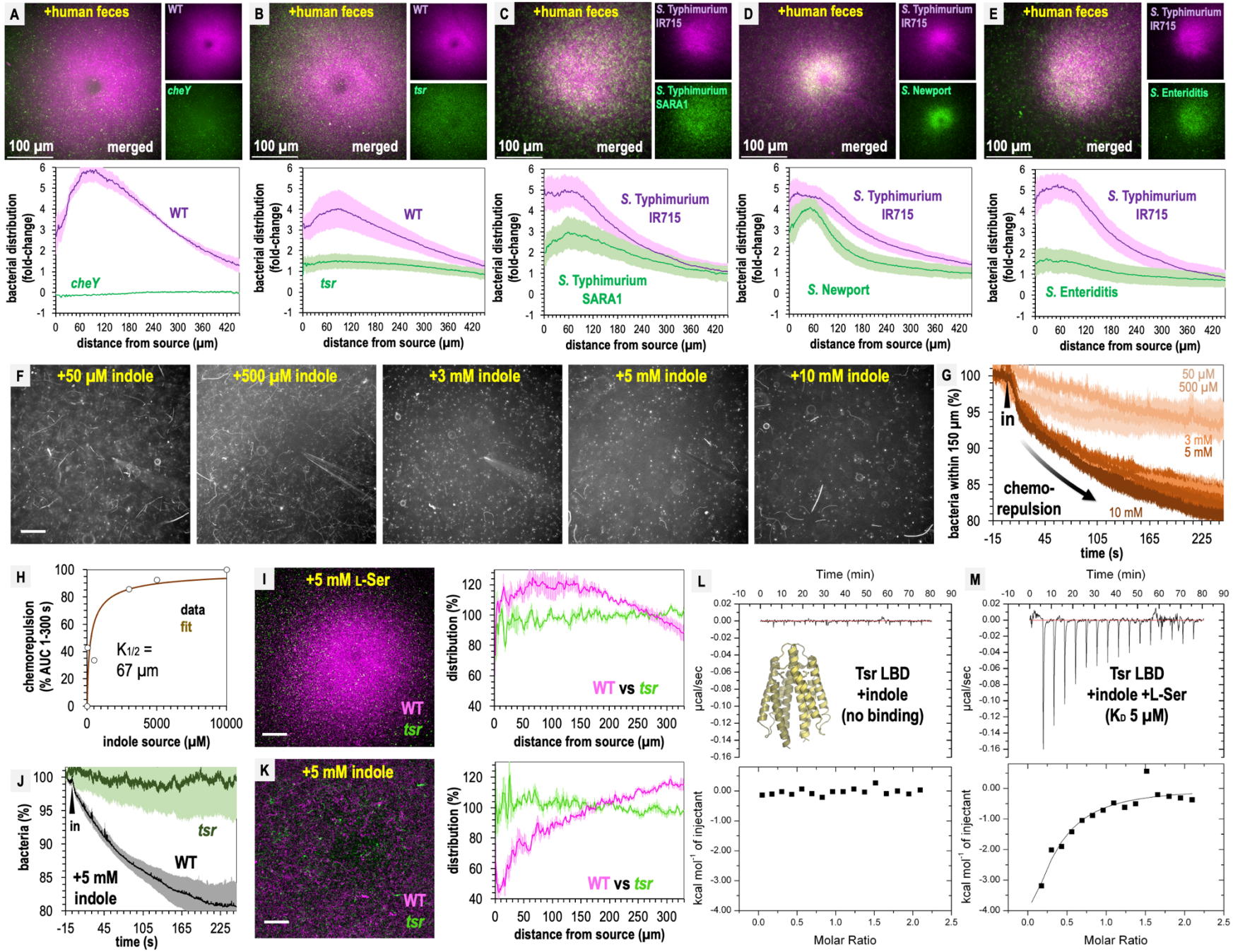
A
+human feces
WT
cheY
100 µm
merged
B
+human feces
WT
tsr
100 µm
merged
C
+human feces
S. Typhimurium IR715
S. Typhimurium SARA1
100 µm
merged
D
+human feces
S. Typhimurium IR715
S. Newport
100 µm
merged
E
+human feces
S. Typhimurium IR715
S. Enteriditis
100 µm
merged
bacterial distribution (fold-change)
distance from source (µm)
WT
cheY
tsr
S. Typhimurium IR715
S. Typhimurium SARA1
S. Newport
S. Enteriditis
F
+50 µM indole
+500 µM indole
+3 mM indole
+5 mM indole
+10 mM indole
G
bacteria within 150 µm (%)
time (s)
in
chemo-repulsion
50 µM
500 µM
3 mM
5 mM
10 mM
H
chemorepulsion (% AUC 1-300 s)
indole source (µM)
data
fit
K1/2 = 67 µm
I
+5 mM L-Ser
WT
tsr
distribution (%)
distance from source (µm)
WT vs tsr
J
bacteria (%)
time (s)
in
tsr
WT
+5 mM indole
K
+5 mM indole
WT
tsr
distribution (%)
distance from source (µm)
WT vs tsr
L
Time (min)
µcal/sec
Tsr LBD +indole (no binding)
kcal mol-1 of injectant
Molar Ratio
M
Time (min)
µcal/sec
Tsr LBD +indole +L-Ser (KD 5 µM)
kcal mol-1 of injectant
Molar Ratio

192

Fig. 3. Fecal indole is insufficient for chemorepulsion but indole in isolation is a strong chemorepellent. A-E. Dual-channel imaging of chemotactic responses to solubilized human feces by WT *S.* Typhimurium IR715 (pink) and isogenic mutants or clinical isolate strains, as indicated. Shown are max projections at time 295-300 s post-treatment. Data are means and error bars are standard error of the mean (SEM, n=3-5). See also Movies S2-S3. F. Representative max projections of responses at 295-300 s of indole treatment. G-H. Quantification of chemorepulsion as a function of indole concentration (n=3-5). I-K. Comparison of WT and *tsr* mutant responses to L-Ser or indole. See also Fig. S2. L-M. Isothermal titration calorimetry (ITC) experiments with 50 μM *S.* Typhimurium Tsr ligand-binding domain (LBD) and indole, or with L-Ser in the presence of 500 μM indole. Data are means and error bars are standard error of the mean (SEM, n=3-5). AUC indicates area under the curve. Scale bars are 100 μm. See also Movies S2-S3.

We compared the chemotactic responses of the WT and *tsr* strains when exposed to sources of these effectors, and found Tsr to be required for both chemorepulsion from indole and chemoattraction to L-Ser (Fig. 3I-K). The canonical mode of chemoreceptor effector recognition involves binding of the effector to the ligand-binding domain (LBD) [7,48], but the mechanism by which indole is sensed through Tsr has not been elucidated. We recently reported the first crystal structure of *S.* Typhimurium Tsr LBD, which clearly defines how the binding site recognizes the L-Ser ligand (PDB code: 8fyv), and we thought it unlikely indole can be accommodated at the same site [24]. Nevertheless, to test whether the Tsr LBD binds indole directly, we expressed and purified the LBD, corresponding to the soluble periplasmic portion, and performed isothermal titration calorimetry (ITC). These data show that no binding occurs between the Tsr LBD and indole (Fig. 3L). We next wondered if indole acts as an allosteric regulator, possibly through interacting with the L-Ser bound form or interfering with L-Ser recognition. To address these possibilities, we performed ITC of 50 μM Tsr LBD with L-Ser in the presence of 500 μM indole and observed a robust exothermic binding curve and K_D of 5 μM, identical to the binding of L-Ser alone (Fig. 3M) [24]. These data indicate that indole does not alter the Tsr LBD affinity for L-Ser.

We conclude that Tsr senses indole through an atypical mechanism, which might either involve regulation through a solute-binding protein [18,49], responsiveness to perturbation in the proton motor force [13], or binding to a different region other than the periplasmic LBD. Our findings reveal that while indole acts as a chemorepellent for *S.* Typhimurium in isolation, sensed through Tsr, its presence within fecal material mixed with other effectors is insufficient to elicit chemorepulsion.

Compromising between conflicting effector signals through chemohalation

Earlier work with *E. coli* revealed that exposure to mixtures of L-Ser and indole can generate

intermediate chemotactic responses between chemoattraction and chemorepulsion after prolonged exposure (1-6 h) (Table S1) [20]. Having confirmed that Tsr in *S.* Typhimurium mediates opposing chemotactic responses to the chemoattractant L-Ser and the chemorepellent indole in isolation, we next sought to learn how the bacterial population behaves when confronted with physiological combinations of these effectors. To address this, we performed a series of CIRA experiments with 500 μM L-Ser and increasing concentrations of indole at L-Ser:indole molar ratios of 10:1, 1:1, or 1:10 (Fig. 4A-D, Movie S4).

These experiments reveal a fascinating transition in the distribution of the pathogen population as a function of increasing chemorepellent, which occurs within minutes of exposure (Fig. 4A-D, Movie S4). With only chemoattractant present, the bacterial population organizes tightly around the effector source (Fig. 4A, Movie S4). When indole is introduced at a concentration 10-fold lower than L-Ser, the bacterial distribution still exhibits chemoattraction but becomes more diffuse (Fig. 4B, Movie S4). At a 1:1 ratio of chemoattractant and chemorepellent, a novel population structure emerges in which the swimming bacteria are attracted toward the source but form a halo around the treatment with an interior region of avoidance (Fig. 4C, Fig. 4E, Movie S4). When the concentration of indole is 10-fold higher than L-Ser, the bacteria exhibit a wider zone of avoidance (Fig. 4D-E, Movie S4). Interestingly, whereas 5 mM indole on its own induces strong chemorepulsion (Fig. S2I, Movie S4), the addition of 10-fold lower L-Ser effectively converts the behavior to a null response (Fig. 4D-E, Movie S4). This demonstrates that even at the highest concentrations of indole *S.* Typhimurium might encounter in the gut, the presence of chemoattractant can override indole chemorepulsion.

The intermediate responses to opposing effector mixtures bear similarities to CIRA experiments with fecal material, some of which also exhibited a halo-like structure around the treatment source (Fig. 2, Movies S2-S3). To our knowledge, there exists no consensus term for intermediate chemotaxis responses of this nature, so here we introduce “chemohalation,” in reference to the halo formed by the cell population, and which is congruent with the established nomenclature of chemoattraction and chemorepulsion. We expect chemohalation is a compromise in positional location at the population level between the chemoattraction driven by L-Ser and the chemorepulsion driven by indole. Across these experiments, the interior zone of avoidance roughly corresponds to where the local concentration of indole exceeds 10 nM (Fig. 4E-F). In a biological setting, we presume that the distribution bias orchestrated by chemohalation regulates the

probability that cells will colonize, adhere, and transition to sessility at a given site; the greater the local indole content, the wider the zone of avoidance and the less likely tissue invasion occurs.

We questioned why non-typhoidal *Salmonella* are attracted to a biological solution with high concentrations of indole, a chemical reported to inhibit bacterial growth [12,50,51]. We examined how bacterial growth is affected by 0-25 mM indole or L-Ser in a background of minimal media (MM). As expected, increasing amounts of the nutrient L-Ser provide a growth advantage for all *Salmonella* strains analyzed, with maximal benefit achieved by approximately 500 µM (Fig. 4G). Equivalent treatments with indole show tolerance up to approximately 1 mM, with growth inhibition occurring in the 1-5 mM range and lethality occurring at indole concentrations greater than 5 mM (Fig. 4H). However, adding L-Ser in a background of 500 µM indole provides only a small growth enhancement (Fig. 4I), and addition of 500 µM L-Ser increases tolerance for indole up to about 1 mM, above which indole toxicity is unavoidable (Fig. 4J). So, we conclude that mixtures of these effectors also impact growth differently than the effectors in isolation, and the relative attraction to combinations of these effectors relates to their propensity to enhance or inhibit growth.

Conclusions

Bacteria in the human gastrointestinal tract encounter complex chemical landscapes that contain both chemoattractants and chemorepellents. However, chemotaxis responses are often studied in isolation, outside of their biological and ecological contexts, which can lead to an over- or underestimation of the roles specific interactions play in natural settings. In the present work, we contribute to an emerging understanding that bacteria exhibit rapid and well-orchestrated responses to conflicting stimuli distinct from chemoattraction or chemorepulsion and relate these chemotactic compromises to enteric infection and pathogen growth (Fig. S3) [20,52]. Previously, no study had addressed whether bacteria other than *E. coli* sense indole as a chemorepellent. In the model system we investigated, we confirm that *S.* Typhimurium utilizes the chemoreceptor Tsr to respond to indole as a chemorepellent and L-Ser as a chemoattractant (Fig. 3). Further, we show that physiological mixtures of these effectors induce the behavior we define here as chemohalation, where the bacteria accumulate at a distance from the treatment source and form a halo with an interior zone of avoidance (Fig. 3, Fig. 4, Fig. S2, Movie S4). Our study is the first to capture real-time videos of this phenomenon for an enteric pathogen and visualize how the population structure

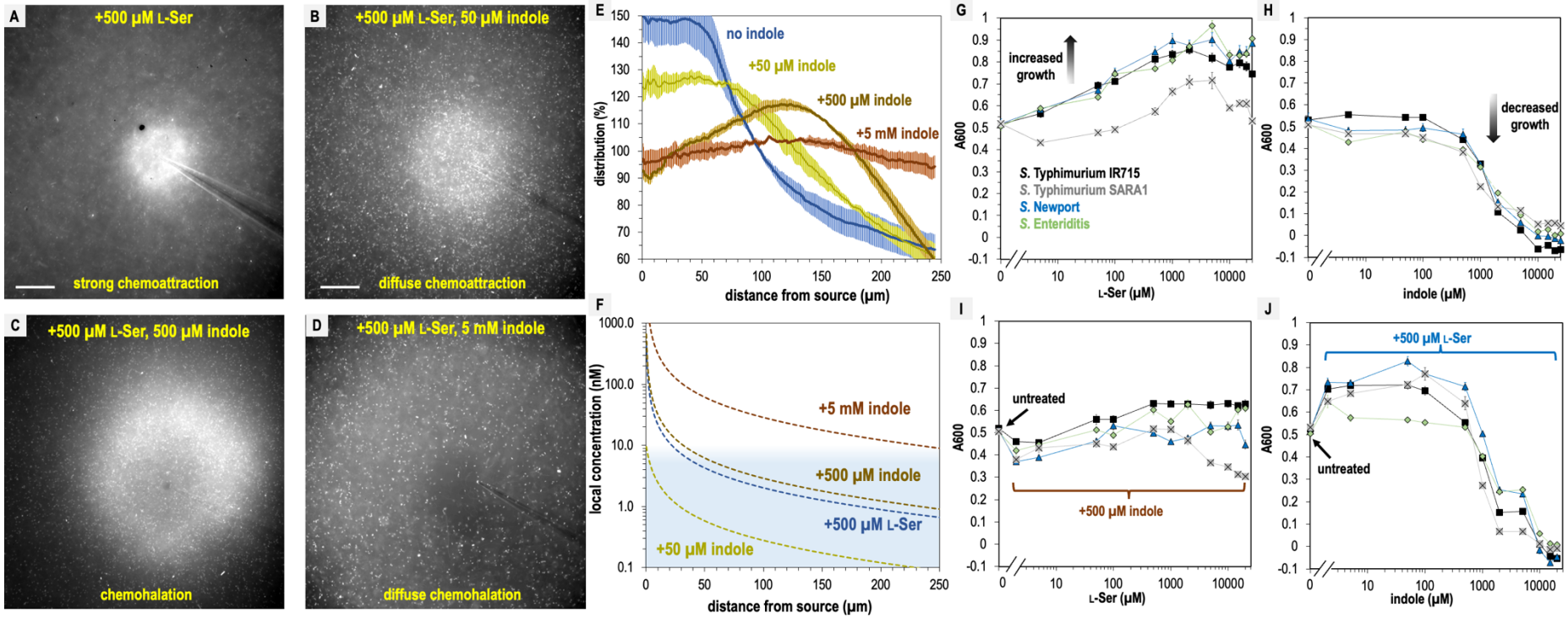

Fig. 4. *S.* Typhimurium mediates distinct chemotactic responses based on the ratio of L-Ser to indole. A-D. Representative max projections of responses to treatments of L-Ser and indole at 295-300 s, as indicated. E. Relative bacterial distribution in response to treatments of 500 µM L-Ser and varying amounts of indole, from panels A-D, with the mean value normalized to 100%. F. Diffusion modeling of local effector concentrations based on sources of 5 mM indole (dark brown), 500 µM L-Ser (blue), 500 µM indole (light brown), and 50 µM indole (yellow) are shown as dashed lines. The approximate local concentration of indole that elicits a transition in chemotactic behavior is highlighted in light blue. Data are means and error bars are standard error of the mean (SEM, n=3-5). Scale bars are 100 µm. G-H. Bacterial growth as a function of L-Ser or indole, at the time point where the untreated culture reaches A_{600} of 0.5. I-J. Bacterial growth +/- pretreatment with 500 µM indole or L-Ser, and increasing concentrations of indole or L-Ser, as indicated at the time point where the untreated culture reaches A_{600} of 0.5. Data are means and error bars are standard error of the mean (SEM, n=8-24). See also Figure S3.

279

280

changes based on the ratio of attractant to repellent, ranging from chemoattraction, diffuse chemoattraction, chemohalation, diffuse chemohalation, and chemorepulsion (Fig. 4, Fig. S2, Fig. S3, Movie S4). These dynamic micron-scale population structures would be difficult or impossible to detect and quantify without directly viewing them through live imaging.

We predicted that human fecal material, rich in indole, would elicit chemorepulsion, inhibit pathogen growth, and protect against infection. Instead, we found that chemotactic sensing of human fecal material promotes colonic invasion, predominantly eliciting chemoattraction or chemohalation (Fig. 1, Fig. S1, Fig. 2, Movies S1-S3). We also found that chemotactic sensing of opposing effectors mediates efficient colonic invasion but provides no advantage when only a single effector is present (Fig. 1, Fig. S1). As evidenced by the phenomenon of chemohalation, the bacteria bias their spatial location based on the ratio of chemoattractant to chemorepellent, and we expect this behavior functions to rank colonization niches and regulate the probability of invading specific sites. In the context of *S.* Typhimurium infection, we propose that Tsr orchestrates a compromise between seeking niches rich in nutrients, signaled by local L-Ser concentrations, and avoiding niches with high microbial competition, indicated by local indole concentrations (Fig. S3). Chemorepulsion from indole can be overridden by the presence of chemoattractants, and *S.* Typhimurium growth is quite tolerant of indole within physiological ranges, suggesting the bacteria generally prioritize nutrient acquisition over the inhibitory effects of indole (Fig. 4). Since the enteric lumen may never be devoid of attractant stimuli, it is possible that outright chemorepulsion from a source of indole may not actually occur *in vivo*.

Having characterized and confirmed the dual sensing role of Tsr for *S.* Typhimurium, we speculate that the diverse bacterial species that possess Tsr orthologues, particularly common among *Enterobacteriaceae* [24], are capable of similar chemohalation behaviors and regulating taxis based on local indole content, further supporting indole as a key regulator of polymicrobial communities of the gut [12,16]. Recently, we reported on *Enterobacteriaceae* chemotactic sensing of blood serum, another complex biological effector source at the host-pathogen interface, and those responses appear to involve chemohalation [24]. Evidence of chemohalation is also seen in the case of the gastric pathogen *Helicobacter pylori* responding to mixtures of urea, a chemoattractant, and acid, a chemorepellent [53,54]. Continuing to investigate chemohalation behaviors and understanding how they coordinate bacterial colonization may provide important insights into how chemotaxis confers fitness advantages in natural environments.

STAR Methods

RESOURCE AVAILABILITY

KEY RESOURCES TABLE

REAGENT or RESOURCE	SOURCE	IDENTIFIER
Bacterial Strains		
S. enterica Typhimurium IR715 nalidixic acid derivative of ATCC 14028	Rivera-Chávez, F. et al.[28]	N/A
S. enterica Typhimurium IR715 Δ*cheY::Tn10* (Tet^R)	Rivera-Chávez, F. et al.[28]	N/A
S. enterica Typhimurium IR715 Δ*tsr::pFR3* (Cm^R)	Rivera-Chávez, F. et al.[28]	N/A
S. enterica SARA1	Beltran, P. et al.[55]	N/A
S. enterica Newport	Shariat, N. et al.[46]	M11018046001A
S. enterica Enteriditis	Shariat, N. et al.[46]	05E01375
E. coli BL21-DE3	Millipore-Sigma	Cat# 70954-3
Biological Samples		
Single Human Donor Fecal Sample	Lee BioSolutions	Cat# 991-18
Chemicals, Peptides, and Recombinant Proteins		
L-Serine	Fisher	Cat# 56-45-1
Indole	Sigma	Cat# I3408-100G
Hydroxylamine hydrochloride	Sigma	Cat# 159417-100G
Recombinant DNA		
pXS-sfGFP	Glenn et al.[24]	N/A
pXS-mPlum	Glenn et al.[24]	N/A
pET-30a(+)-SeTsrLBD	Glenn et al.[24]	N/A
Software and Algorithms		
Matlab R2022a	The MathWorks Inc., Natick, Massachusetts, USA	Mathworks.com
Fiji	ImageJ, Bethesda, Maryland, USA[56]	Fiji Home
TrackingGUI_rp	R. Parthasarathy [57]	TrackingGUI Public

Lead contact

Further information and requests for resources and reagents should be directed to and will be fulfilled by the lead contact, Arden Baylink (arden.baylink@wsu.edu).

Materials availability

Strains and plasmids generated in this study will be made available upon request by the Lead Contact with a completed Materials Transfer Agreement.

Data availability

Source data from this work are archived and available upon request by the Lead Contact. This paper does not report original code. Any additional information required to reanalyze the data reported in this paper is available from the lead contact upon request.

EXPERIMENTAL MODEL AND STUDY DETAILS

All methods were carried out in accordance with relevant guidelines, regulations, and state and federal law. Experimental protocols were approved by the Institutional Biosafety Committee (IBC) of Washington State University (#1372).

Bacterial strains and growth conditions

Bacterial strains and plasmids used in this study are listed in Table 1. As previously described [24], bacteria intended for chemotaxis assays were grown overnight in tryptone broth (TB) with antibiotic selection, as appropriate. Motile bacteria were prepared with a 1:1000 back-dilution and grown shaking for approximately 4 hours at 37˚ C to reach A_{600} of 0.5. Cells were centrifuged, washed, and resuspended in a chemotaxis buffer (CB) containing 10 mM potassium phosphate (pH 7), 10 mM sodium lactate, and 100 µM EDTA to A_{600} of 0.2 and rocked gently at room temperature until fully motile. For *in vitro* growth analyses, cultures were grown overnight in Lysogeny Broth (LB) at 37˚ C. Subsequently, 5 µl of A_{600} 2.0 cells were used to inoculate 200 µl of minimal media (MM), containing 47 mM Na_2HPO_4, 22 mM KH_2PO_4, 8 mM NaCl, 2mM $MgSO_4$, 0.4% glucose (w/v) 11.35 mM $(NH_4)_2SO_4$, 100 µM $CaCl_2$ and L-Ser and/or indole at the described concentrations, and cultured in a 96-well microtiter plate. Cultures were grown at 37˚ C and monitored by A_{600} readings at 5-minute intervals.

METHOD DETAILS

Chemosensory injection rig assay (CIRA)

CIRA was performed as described previously [24]. Briefly, an Eppendorf Femtotip 2 microcapillary containing the treatment of interest was lowered into a pond of 50 µl of motile cells using a Sutter micromanipulator. An injection flow of effector into the pond at approximately 300 fl per minute was achieved using a Femtojet 4i set to P_c 35. Solubilized fecal treatments were prepared by

dissolving 1 g of commercially obtained human feces (Innovative Research) in 10 ml of CB. The solution was clarified by centrifugation at 10,000 g for 20 minutes, followed by sterile filtration through a 0.2 µm filter. Treatment solutions of indole and L-Ser were also diluted into CB and sterile-filtered before application. Videos were recorded using an inverted Nikon Ti2 microscope with heated sample chamber at 37 ˚C.

CIRA microgradient modeling

Modeling the microgradient generated through CIRA was performed as described earlier [24], based on the continual injection and diffusion of an effector from a fixed-point source. Briefly, diffusion is modeled as a 3D process where the diffusing substance is gradually and continuously introduced at a fixed point within a large surrounding fluid volume. The substance is prepared at a concentration of M_s (typically between 0.5 µM and 5 mM) and injected at a volume rate of Q = 305.5 fl/min. The species then diffuses into the ambient fluid with a diffusion constant D.

$$C(r,t) = \frac{q}{4\pi Dr} erfc \frac{r}{2\sqrt{Dt}}$$

Here, r is the distance from the point source, t is the time from initial injections, q is the injection rate of the species (equal to M_sQ), and C is the species concentration.

Purification of recombinant S. Typhimurium Tsr LBD

Purification of *S.* Typhimurium Tsr LBD was performed as described previously [24]. Rosetta BL21(DE3) *E. coli* cells with a Tsr-LBD-pet-30a(+) vector were grown with LB and 20 µg kanamycin and induced at A_{600} of 0.8 with 0.4 mM isopropyl β-D-1-thiogalactopyranoside (IPTG). Cells were harvested after 3 h of growth at 37˚ C. Cells were lysed, the lysate was clarified through centrifugation, and the soluble fraction was subjected to an ammonium sulfate precipitation, with Tsr LBD precipitating in the 20-40% fraction. The fractions were pooled, treated with TEV protease to remove the N-terminal expression sequence, and purified using an anion exchange column and Akta FPLC. Lastly, the protein was purified by gel filtration using an S200 column with a final buffer of 50 mM Tris pH 7.5, 1 mM EDTA, and 150 mM NaCl and stored at 7 mg/ml at -80 C.

Isothermal titration calorimetry ligand binding studies (ITC)

ITC experiments were performed using a Microcal ITC200 instrument (GE Healthcare). Either 500 μM indole or L-Ser was titrated in 2.5 μL injections into a 200 μL sample cell containing 50 μM Tsr LBD. For the indole/L-Ser competition experiment, 500 μM indole was added to both the titrant and sample cell, thus providing a constant excess background concentration of indole. For all experimental conditions, blank titrations were also collected in which indole or L-Ser was titrated into a cell containing buffer alone. All experiments were performed using thoroughly degassed samples at 25 °C in 50 mM Tris, 150 mM NaCl, 1 mM EDTA, pH 7.5. The reference power was set to 5 μcal/sec. The resulting power curves were integrated using the Origin analysis software included with the instrument. The heat of dilution was subtracted from each point using the blank. A single-site binding model was then fit to the data, floating parameters describing the binding enthalpy (ΔH), equilibrium constant (K_D), and apparent binding stoichiometry (n). The instrument software was used for this purpose.

Quantification of indole and serine in human fecal samples

Solubilized human feces was prepared as described above for CIRA and analyzed by mass spectrometry to determine the molar serine content as a service through the University of Washington Mass Spectrometry Center. This measurement reflects total serine, of which close to 100% is expected to be L-Ser [24]. As described in earlier work, the indole content of solubilized human fecal samples was determined using a hydroxylamine-based calorimetric assay with purified indole as a reference and standard [58].

Explant infection assays

Swine intestinal tissue was acquired from the descending colon of an 8-week-old animal, pursuant to animal protocol ASAF #7128, approved through the Washington State University IACUC. Before infection, the luminal side of an approximately 20 by 20 mm piece of swine intestinal explant tissue was gently washed with PBS to remove fecal matter. Next, the tissue section was bathed in 2 ml of chemoeffector solution (solubilized human fecal matter, a mixture of 338 μM L-Ser and 862 μM indole, 338 μM L-Ser alone, or 862 μM indole alone) in a 6-well tissue culture plate (Celltreat) and incubated at 4° C for 1 h. Then, tissue was transferred to a 35 mm Mattek dish where the luminal side of the tissue was exposed to a bacterial solution containing a 1:1 mixture

(10^9 CFU each) of WT *S.* Typhimurium IR715 and either the isogenic *tsr* or *cheY* mutant, suspended in CB at a volume of 300 µl. The tissue was then incubated in the dish with the competing bacteria at 37 °C and 5% CO_2 for 1-, 3-, or 6-h. After, half of the tissue was transferred into screwcap tubes containing 500 µl LB media and 5-10 2.3 mm zirconia beads (BioSpec Products) on ice and homogenized using a Bead Mill 24 (Fisher Scientific, 6.5 m/s for 60 s, four times). To enumerate the intracellular bacteria, the other half of the tissue was washed in PBS and incubated in PBS containing 100 g/ml gentamicin for 1 h at 37 °C and 5% CO_2, then washed twice in PBS, as done previously [39,59,60]. The homogenization process was then repeated for the gentamicin-treated tissue. CFUs were enumerated by 100 µl spot plating of 10-fold dilutions on LB agar plates containing the appropriate antibiotic [39,61]. Competitive index values were calculated by dividing the number of mutant CFUs by the number of WT CFUs for each treatment and time point [62,63].

QUANTIFICATION AND STATISTICAL ANALYSIS

Quantification of CIRA data

Videos of chemotactic responses were quantified as described previously [24]. The number of cells in each frame was calculated by determining a fluorescence intensity ratio per cell for frames pre-treatment and extrapolated using the 'plot profile' function of ImageJ. The distribution of the bacteria was calculated using the Radial Profile ImageJ plugin. Local background subtraction was performed based on experiments with the non-chemotactic *cheY* strain to control for autofluorescence in solubilized fecal samples.

Statistical Analyses

Competitive indices (CIs) for explant experiments were calculated for each treatment group at each time point. Log-transformed CI values were obtained by taking the logarithm ($\log_{10}$) of the original CI measurements. These log-transformed values were then subjected to statistical analysis. First, a one-sample t-test was performed to determine whether the mean of the log-transformed CIs significantly differed from zero. In cases where the assumption of normality was violated, the non-parametric Wilcoxon rank sum test was applied as an alternative. Effect size was assessed using Cohen's *d and* calculated using the same log-transformed CIs.

The formula for Cohen's *d* value is as follows:

$$d = \frac{\mathrm{M}_1 - \mathrm{M}_2}{\sigma_{\mathrm{pooled}}}$$

Where M_1 serves as the mean of the treatment group, M_2 serves as the mean of the control group, and σ_{pooled} is the pooled standard deviation:

$$\sigma_{pooled} = \sqrt{\frac{{\sigma_1}^2 + {\sigma_2}^2}{2}}$$

Here, σ_1 is the standard deviation of the treatment group, and σ_2 is the standard deviation of the control group.

Acknowledgments

Funding for this research was provided by NIAID through awards 1K99AI148587 and 4R00AI148587-03, and funding from Washington State University to AB. Bacterial strains were provided by Nikki Shariat (University of Georgia, Athens), Nkuchia Mikanatha and Pennsylvania NARMS and GenomeTrakr Programs, and Andreas Bäumler (University of California, Davis). All research on human samples was performed in accordance with, and approval of, the Institutional Biosafety Committee and Institutional Animal Care and Use Committee at Washington State University.

Author Contributions

K.F. performed the microgradient modeling and explant experiments. A.B. conducted the CIRA experiments and purification of Tsr-LBD. Z.G. performed bacterial growth experiments. M.S. and M.J.H. performed the ITC experiments. All authors contributed to data analyses and writing of the manuscript.

Declaration of Interests

A.B. owns Amethyst Antimicrobials, LLC.

Declaration of generative AI and AI-assisted technologies in the writing process

During the preparation of this work the authors used ChatGPT in order to proof-read and enhance the clarity and organization of the text. After using this tool/service, the authors reviewed and edited the content as needed and take full responsibility for the content of the published article.

Supplemental Information

Document S1. Table S1 and Figures S1–S3.

Movie S1. Chemotactic response of *S.* Typhimurium IR715 to solubilized human feces, related to Figure 2. Representative CIRA experiments showing *S.* Typhimurium IR715 WT and mutant strains responding to a source over 300 s (shown at 10x speed) Viewable at: https://www.youtube.com/watch?v=BqUcRN3YwjU

Movie S2. Chemotactic response of *S.* Typhimurium IR715 WT and chemotactic mutant strains to solubilized human feces, related to Figure 3. Representative CIRA experiments showing competition between *S.* Typhimurium IR715 (mPlum) and *cheY*, or *tsr*, as indicated (GFP), over 300 s. Viewable at: https://www.youtube.com/watch?v=D5JL46b4lsI

Movie S3. Chemotactic response of *S. enterica* clinical isolates to solubilized human feces, related to Figure 3. Representative CIRA experiments showing competition between *S.* Typhimurium IR715 (mPlum) and clinical isolates, as indicated (GFP), responding to a source of solubilized human feces over 300 s. Viewable at: https://www.youtube.com/watch?v=dLsFDV0XgpY

Movie S4. Chemotactic response of *S.* Typhimurium IR715 to L-Ser and indole treatments, related to Figure 4 and Figure S2. Representative CIRA experiments with treatment sources as indicated, over 300 s. Viewable at: https://www.youtube.com/watch?v=bNQMqF2QMek

References

1. Zhou, B., Szymanski, C.M., and Baylink, A. (2023). Bacterial chemotaxis in human diseases. Trends in Microbiology *31*, 453–467. https://doi.org/10.1016/j.tim.2022.10.007.

2. Keegstra, J.M., Carrara, F., and Stocker, R. (2022). The ecological roles of bacterial chemotaxis. Nature Reviews Microbiology. https://doi.org/10.1038/s41579-022-00709-w.

3. Bi, S., and Sourjik, V. (2018). Stimulus sensing and signal processing in bacterial chemotaxis. Current Opinion in Microbiology *45*, 22–29. https://doi.org/10.1016/j.mib.2018.02.002.

4. Matilla, M.A., and Krell, T. (2018). The effect of bacterial chemotaxis on host infection and pathogenicity. FEMS Microbiology Reviews *42*. https://doi.org/10.1093/femsre/fux052.

5. Matilla, M.A., Gavira, J.A., and Krell, T. (2023). Accessing nutrients as the primary benefit arising from chemotaxis. Current Opinion in Microbiology *75*, 102358. https://doi.org/10.1016/j.mib.2023.102358.

6. Matilla, M.A., and Krell, T. (2017). Chemoreceptor-based signal sensing. Current Opinion in Biotechnology *45*, 8–14. https://doi.org/10.1016/j.copbio.2016.11.021.

7. Ortega, Á., Zhulin, I.B., and Krell, T. (2017). Sensory Repertoire of Bacterial Chemoreceptors. Microbiol Mol Biol Rev *81*, e00033-17. https://doi.org/10.1128/MMBR.00033-17.

8. Rogers, A.W.L., Tsolis, R.M., and Bäumler, A.J. (2020). Salmonella versus the Microbiome. Microbiology and Molecular Biology Reviews *85*, e00027-19. https://doi.org/10.1128/MMBR.00027-19.

9. Vos, W.M. de, Tilg, H., Hul, M.V., and Cani, P.D. (2022). Gut microbiome and health: mechanistic insights. Gut *71*, 1020–1032. https://doi.org/10.1136/gutjnl-2021-326789.

10. Hill, J.H., Massaquoi, M.S., Sweeney, E.G., Wall, E.S., Jahl, P., Bell, R., Kallio, K., Derrick, D., Murtaugh, L.C., Parthasarathy, R., et al. (2022). BefA, a microbiota-secreted membrane disrupter, disseminates to the pancreas and increases β cell mass. Cell Metabolism *34*, 1779-1791.e9. https://doi.org/10.1016/j.cmet.2022.09.001.

11. Li, X., Zhang, B., Hu, Y., and Zhao, Y. (2021). New Insights Into Gut-Bacteria-Derived Indole and Its Derivatives in Intestinal and Liver Diseases. Front. Pharmacol. *12*, 769501. https://doi.org/10.3389/fphar.2021.769501.

12. Lee, J.-H., and Lee, J. (2010). Indole as an intercellular signal in microbial communities. FEMS Microbiol Rev *34*, 426–444. https://doi.org/10.1111/j.1574-6976.2009.00204.x.

13. Gupta, R., Rhee, K.Y., Beagle, S.D., Chawla, R., Perdomo, N., Lockless, S.W., and Lele, P.P. (2022). Indole modulates cooperative protein–protein interactions in the flagellar motor. PNAS Nexus *1*, pgac035. https://doi.org/10.1093/pnasnexus/pgac035.

14. Darkoh, C., Chappell, C., Gonzales, C., and Okhuysen, P. (2015). A Rapid and Specific Method for the Detection of Indole in Complex Biological Samples. Appl Environ Microbiol *81*, 8093–8097. https://doi.org/10.1128/AEM.02787-15.

15. Chappell, C.L., Darkoh, C., Shimmin, L., Farhana, N., Kim, D.-K., Okhuysen, P.C., and Hixson, J. (2016). Fecal Indole as a Biomarker of Susceptibility to Cryptosporidium Infection. Infect Immun *84*, 2299–2306. https://doi.org/10.1128/IAI.00336-16.

16. Ye, X., Li, H., Anjum, K., Zhong, X., Miao, S., Zheng, G., Liu, W., and Li, L. (2022). Dual Role of Indoles Derived From Intestinal Microbiota on Human Health. Front. Immunol. *13*, 903526. https://doi.org/10.3389/fimmu.2022.903526.

17. Kumar, A., and Sperandio, V. (2019). Indole Signaling at the Host-Microbiota-Pathogen Interface. mBio *10*, e01031-19. https://doi.org/10.1128/mBio.01031-19.

18. Yang, J., Chawla, R., Rhee, K.Y., Gupta, R., Manson, M.D., Jayaraman, A., and Lele, P.P. (2020). Biphasic chemotaxis of *Escherichia coli* to the microbiota metabolite indole. Proc. Natl. Acad. Sci. U.S.A. *117*, 6114–6120. https://doi.org/10.1073/pnas.1916974117.

19. Bansal, T., Englert, D., Lee, J., Hegde, M., Wood, T.K., and Jayaraman, A. (2007). Differential Effects of Epinephrine, Norepinephrine, and Indole on *Escherichia coli* O157:H7 Chemotaxis, Colonization, and Gene Expression. Infect Immun *75*, 4597–4607. https://doi.org/10.1128/IAI.00630-07.

20. Livne, N., and Vaknin, A. (2022). Collective responses of bacteria to a local source of conflicting effectors. Sci Rep *12*, 4928. https://doi.org/10.1038/s41598-022-08762-4.

21. Englert, D.L., Manson, M.D., and Jayaraman, A. (2009). Flow-Based Microfluidic Device for Quantifying Bacterial Chemotaxis in Stable, Competing Gradients. Appl Environ Microbiol *75*, 4557–4564. https://doi.org/10.1128/AEM.02952-08.

22. Adler, J., and Tso, W.-W. (1974). "Decision"-Making in Bacteria: Chemotactic Response of *Escherichia coli* to Conflicting Stimuli. Science *184*, 1292–1294. https://doi.org/10.1126/science.184.4143.1292.

23. Kohli, N., Crisp, Z., Riordan, R., Li, M., Alaniz, R.C., and Jayaraman, A. (2018). The microbiota metabolite indole inhibits Salmonella virulence: Involvement of the PhoPQ two-component system. PLOS ONE *13*, e0190613. https://doi.org/10.1371/journal.pone.0190613.

24. Glenn, S.J., Gentry-Lear, Z., Shavlik, M., Harms, M.J., Asaki, T.J., and Baylink, A. (2024). Bacterial vampirism mediated through taxis to serum. eLife *12*, RP93178. https://doi.org/10.7554/eLife.93178.3.

25. Piñas, G.E., DeSantis, M.D., Cassidy, C.K., and Parkinson, J.S. (2022). Hexameric rings of the scaffolding protein CheW enhance response sensitivity and cooperativity in Escherichia coli chemoreceptor arrays. Science Signaling *15*, eabj1737. https://doi.org/10.1126/scisignal.abj1737.

26. Burt, A., Cassidy, C.K., Ames, P., Bacia-Verloop, M., Baulard, M., Huard, K., Luthey-Schulten, Z., Desfosses, A., Stansfeld, P.J., Margolin, W., et al. (2020). Complete structure of the chemosensory array core signalling unit in an E. coli minicell strain. Nat Commun *11*, 743. https://doi.org/10.1038/s41467-020-14350-9.

27. Winter, S.E., Lopez, C.A., and Bäumler, A.J. (2013). The dynamics of gut-associated microbial communities during inflammation. EMBO Reports *14*, 319–327. https://doi.org/10.1038/embor.2013.27.

582 28. Rivera-Chávez, F., Winter, S.E., Lopez, C.A., Xavier, M.N., Winter, M.G., Nuccio, S.-P.,
583 Russell, J.M., Laughlin, R.C., Lawhon, S.D., Sterzenbach, T., et al. (2013). Salmonella Uses
584 Energy Taxis to Benefit from Intestinal Inflammation. PLoS Pathog *9*, e1003267.
585 https://doi.org/10.1371/journal.ppat.1003267.

586 29. Winter, S.E., Thiennimitr, P., Winter, M.G., Butler, B.P., Huseby, D.L., Crawford, R.W.,
587 Russell, J.M., Bevins, C.L., Adams, L.G., Tsolis, R.M., et al. (2010). Gut inflammation
588 provides a respiratory electron acceptor for Salmonella. Nature *467*, 426–429.
589 https://doi.org/10.1038/nature09415.

590 30. Cooper, K.G., Chong, A., Kari, L., Jeffrey, B., Starr, T., Martens, C., McClurg, M., Posada,
591 V.R., Laughlin, R.C., Whitfield-Cargile, C., et al. (2021). Regulatory protein HilD stimulates
592 Salmonella Typhimurium invasiveness by promoting smooth swimming via the methyl-
593 accepting chemotaxis protein McpC. Nat Commun *12*, 348. https://doi.org/10.1038/s41467-
594 020-20558-6.

595 31. Vega, N.M., Allison, K.R., Samuels, A.N., Klempner, M.S., and Collins, J.J. (2013).
596 *Salmonella typhimurium* intercepts *Escherichia coli* signaling to enhance antibiotic
597 tolerance. Proc. Natl. Acad. Sci. U.S.A. *110*, 14420–14425.
598 https://doi.org/10.1073/pnas.1308085110.

599 32. Roager, H.M., and Licht, T.R. (2018). Microbial tryptophan catabolites in health and disease.
600 Nat Commun *9*, 3294. https://doi.org/10.1038/s41467-018-05470-4.

601 33. Kronsteiner, B., Bassaganya-Riera, J., Philipson, C., Viladomiu, M., Carbo, A., Pedragosa,
602 M., Vento, S., and Hontecillas, R. (2013). Helicobacter pylori Infection in a Pig Model Is
603 Dominated by Th1 and Cytotoxic CD8 $^{+}$ T Cell Responses. Infect Immun *81*, 3803–3813.
604 https://doi.org/10.1128/IAI.00660-13.

605 34. Smith, A.C., and Swindle, M.M. (2006). Preparation of Swine for the Laboratory. ILAR
606 Journal *47*, 358–363. https://doi.org/10.1093/ilar.47.4.358.

607 35. Poutahidis, T., Tsangaris, T., Kanakoudis, G., Vlemmas, I., Iliadis, N., and Sofianou, D.
608 (2001). *Helicobacter pylori* -induced Gastritis in Experimentally Infected Conventional
609 Piglets. Vet Pathol *38*, 667–678. https://doi.org/10.1354/vp.38-6-667.

610 36. Boyen, F., Pasmans, F., Van Immerseel, F., Donné, E., Morgan, E., Ducatelle, R., and
611 Haesebrouck, F. (2009). Porcine *in vitro* and *in vivo* models to assess the virulence of
612 *Salmonella enterica* serovar Typhimurium for pigs. Lab Anim *43*, 46–52.
613 https://doi.org/10.1258/la.2007.007084.

614 37. Boyen, F., Haesebrouck, F., Vanparys, A., Volf, J., Mahu, M., Van Immerseel, F., Rychlik,
615 I., Dewulf, J., Ducatelle, R., and Pasmans, F. (2008). Coated fatty acids alter virulence
616 properties of Salmonella Typhimurium and decrease intestinal colonization of pigs.
617 Veterinary Microbiology *132*, 319–327. https://doi.org/10.1016/j.vetmic.2008.05.008.

38. MacBeth, K.J., and Lee, C.A. (1993). Prolonged inhibition of bacterial protein synthesis abolishes Salmonella invasion. Infect Immun *61*, 1544–1546. https://doi.org/10.1128/iai.61.4.1544-1546.1993.

39. Sharma, A., and Puhar, A. (2019). Gentamicin Protection Assay to Determine the Number of Intracellular Bacteria during Infection of Human TC7 Intestinal Epithelial Cells by Shigella flexneri. BIO-PROTOCOL *9*. https://doi.org/10.21769/BioProtoc.3292.

40. Kitamoto, S., Alteri, C.J., Rodrigues, M., Nagao-Kitamoto, H., Sugihara, K., Himpsl, S.D., Bazzi, M., Miyoshi, M., Nishioka, T., Hayashi, A., et al. (2020). Dietary l-serine confers a competitive fitness advantage to Enterobacteriaceae in the inflamed gut. Nature Microbiology *5*, 116–125. https://doi.org/10.1038/s41564-019-0591-6.

41. Sugihara, K., and Kamada, N. (2020). THE ROLE OF DIETARY L-SERINE IN THE REGULATION OF INTESTINAL MUCUS BARRIER DURING INFLAMMATION. Inflammatory Bowel Diseases *26*, S42–S42. https://doi.org/10.1093/ibd/zaa010.110.

42. Ranque, C.L., Stroble, C., Amicucci, M.J., Tu, D., Diana, A., Rahmannia, S., Suryanto, A.H., Gibson, R.S., Sheng, Y., Tena, J., et al. (2020). Examination of Carbohydrate Products in Feces Reveals Potential Biomarkers Distinguishing Exclusive and Nonexclusive Breastfeeding Practices in Infants. J Nutr *150*, 1051–1057. https://doi.org/10.1093/jn/nxaa028.

43. Ke, Z., Lu, Z., Li, Q., and Tong, W. (2024). Intestinal glucose excretion: A potential mechanism for glycemic control. Metabolism *152*, 155743. https://doi.org/10.1016/j.metabol.2023.155743.

44. Larke, J.A., Bacalzo, N., Castillo, J.J., Couture, G., Chen, Y., Xue, Z., Alkan, Z., Kable, M.E., Lebrilla, C.B., Stephensen, C.B., et al. (2023). Dietary Intake of Monosaccharides from Foods is Associated with Characteristics of the Gut Microbiota and Gastrointestinal Inflammation in Healthy US Adults. The Journal of Nutrition *153*, 106–119. https://doi.org/10.1016/j.tjnut.2022.12.008.

45. Shen, X., Jain, A., Aladelokun, O., Yan, H., Gilbride, A., Ferrucci, L.M., Lu, L., Khan, S.A., and Johnson, C.H. (2022). Asparagine, colorectal cancer, and the role of sex, genes, microbes, and diet: A narrative review. Front Mol Biosci *9*, 958666. https://doi.org/10.3389/fmolb.2022.958666.

46. Shariat, N., Kirchner, M.K., Sandt, C.H., Trees, E., Barrangou, R., and Dudley, E.G. (2013). Subtyping of Salmonella enterica Serovar Newport Outbreak Isolates by CRISPR-MVLST and Determination of the Relationship between CRISPR-MVLST and PFGE Results. J Clin Microbiol *51*, 2328–2336. https://doi.org/10.1128/JCM.00608-13.

47. Ferrari, R.G., Rosario, D.K.A., Cunha-Neto, A., Mano, S.B., Figueiredo, E.E.S., and Conte-Junior, C.A. (2019). Worldwide Epidemiology of *Salmonella* Serovars in Animal-Based Foods: a Meta-analysis. Appl Environ Microbiol *85*, e00591-19. https://doi.org/10.1128/AEM.00591-19.

48. Gavira, J.A., Gumerov, V.M., Rico-Jiménez, M., Petukh, M., Upadhyay, A.A., Ortega, A., Matilla, M.A., Zhulin, I.B., and Krell, T. (2020). How Bacterial Chemoreceptors Evolve Novel Ligand Specificities. mBio *11*, e03066-19. https://doi.org/10.1128/mBio.03066-19.

49. Matilla, M.A., Ortega, Á., and Krell, T. (2021). The role of solute binding proteins in signal transduction. Computational and Structural Biotechnology Journal *19*, 1786–1805. https://doi.org/10.1016/j.csbj.2021.03.029.

50. Chimerel, C., Field, C.M., Piñero-Fernandez, S., Keyser, U.F., and Summers, D.K. (2012). Indole prevents Escherichia coli cell division by modulating membrane potential. Biochim Biophys Acta *1818*, 1590–1594. https://doi.org/10.1016/j.bbamem.2012.02.022.

51. Melander, R.J., Minvielle, M.J., and Melander, C. (2014). Controlling bacterial behavior with indole-containing natural products and derivatives. Tetrahedron *70*, 6363–6372. https://doi.org/10.1016/j.tet.2014.05.089.

52. Moore, J.P., Kamino, K., Kottou, R., Shimizu, T.S., and Emonet, T. (2024). Signal integration and adaptive sensory diversity tuning in *Escherichia coli* chemotaxis. Cell Systems *15*, 628-638.e8. https://doi.org/10.1016/j.cels.2024.06.003.

53. Huang, J.Y., Sweeney, E.G., Sigal, M., Zhang, H.C., Remington, S.J., Cantrell, M.A., Kuo, C.J., Guillemin, K., and Amieva, M.R. (2015). Chemodetection and Destruction of Host Urea Allows Helicobacter pylori to Locate the Epithelium. Cell Host & Microbe *18*, 147–156. https://doi.org/10.1016/j.chom.2015.07.002.

54. Huang, J.Y., Sweeney, E.G., Guillemin, K., and Amieva, M.R. (2017). Multiple Acid Sensors Control Helicobacter pylori Colonization of the Stomach. PLOS Pathogens *13*, e1006118. https://doi.org/10.1371/journal.ppat.1006118.

55. Beltran, P., Plock, S.A., Smith, N.H., Whittam, T.S., Old, D.C., and Selander, R.K. (1991). Reference collection of strains of the Salmonella typhimurium complex from natural populations. Journal of General Microbiology *137*, 601–606. https://doi.org/10.1099/00221287-137-3-601.

56. Schindelin, J., Arganda-Carreras, I., Frise, E., Kaynig, V., Longair, M., Pietzsch, T., Preibisch, S., Rueden, C., Saalfeld, S., Schmid, B., et al. (2012). Fiji: an open-source platform for biological-image analysis. Nat Methods *9*, 676–682. https://doi.org/10.1038/nmeth.2019.

57. Parthasarathy, R. (2012). Rapid, accurate particle tracking by calculation of radial symmetry centers. Nat Methods *9*, 724–726. https://doi.org/10.1038/nmeth.2071.

58. Sugihara, K., Kitamoto, S., Saraithong, P., Nagao-Kitamoto, H., Hoostal, M., McCarthy, C., Rosevelt, A., Muraleedharan, C.K., Gillilland, M.G., Imai, J., et al. (2022). Mucolytic bacteria license pathobionts to acquire host-derived nutrients during dietary nutrient restriction. Cell Reports *40*, 111093. https://doi.org/10.1016/j.celrep.2022.111093.

692 59. Chandra, K. (2022). Gentamicin Protection assay (Intracellular Survival Assay) for
693 Salmonella Typhimurium/Typhi v1. Preprint,
694 https://doi.org/10.17504/protocols.io.b4zmqx46
695 https://doi.org/10.17504/protocols.io.b4zmqx46.

696 60. Rivera Calo, J., Rubinelli, P.M., and Ricke, S.C. (2024). Gentamicin Susceptibility and
697 Comparison of Adhesion and Invasion of Caco-2 and HD11 Cell Lines by Salmonella
698 enterica Serotypes. Applied Sciences *14*, 3305. https://doi.org/10.3390/app14083305.

699 61. Ben-David, A., and Davidson, C.E. (2014). Estimation method for serial dilution
700 experiments. Journal of Microbiological Methods *107*, 214–221.
701 https://doi.org/10.1016/j.mimet.2014.08.023.

702 62. Macho, A.P., Zumaquero, A., Ortiz-Martín, I., and Beuzón, C.R. (2007). Competitive index
703 in mixed infections: a sensitive and accurate assay for the genetic analysis of *Pseudomonas*
704 *syringae* –plant interactions. Molecular Plant Pathology *8*, 437–450.
705 https://doi.org/10.1111/j.1364-3703.2007.00404.x.

706 63. Auerbuch, V., Lenz, L.L., and Portnoy, D.A. (2001). Development of a competitive index
707 assay to evaluate the virulence of Listeria monocytogenes actA mutants during primary and
708 secondary infection of mice. Infect Immun *69*, 5953–5957.
709 https://doi.org/10.1128/IAI.69.9.5953-5957.2001.

710